Available online at www.sciencedirect.com
SCIENCE DIRECT
Thermochimica Acta 440 (2006) 181–187
thermochimica acta
www.elsevier.com/locate/tca

Thermal analysis study of 5,10,15,20-tetrakis (methoxyphenyl) porphyrins and their nickel complexes

Xiuhua Wei [a], Xiuhong Du [b], Donghua Chen [a,*], Zhangping Chen [b]

[a] *Hubei Key Laboratory for Catalysis and Material Science, College of Chemistry and Material Science, South-Central University for Nationalities, Wuhan 430074, Hubei, PR China*
[b] *College of Chemistry and Molecular Science, Wuhan University, Wuhan 430072, Hubei, PR China*

Received 23 June 2005; received in revised form 12 September 2005; accepted 31 October 2005
Available online 7 December 2005

Abstract

The thermal stability in air of 5,10,15,20-tetrakis (4-methoxyphenyl) porphyrin (4-TMPP), 5,10,15,20-tetrakis (3-methoxyphenyl) porphyrin (3-TMPP), and their nickel metallo-complexes (4-TMPP-Ni and 3-TMPP-Ni) has been investigated by thermogravimetry (TG). 4-TMPP and 4-TMPP-Ni exhibit higher thermal stability compared to 3-TMPP and 3-TMPP-Ni. Nickel complexes exhibit a little higher thermal stability than the corresponding porphyrins. The thermal behavior including melting temperature and enthalpy of fusion was determined by differential scanning calorimetry (DSC) and infrared spectra (IR). The activation energies of thermal decompositions of 4-TMPP-Ni and 3-TMPP-Ni were obtained by integral model-free method; the mechanism functions and pre-exponential factors were determined by master plots method. The kinetic models follow the same mechanism function, Avramie-Erofeev equations with integral forms $g(\alpha) = [-\ln(1-\alpha)]^{0.278}$ and $g(\alpha) = [-\ln(1-\alpha)]^{0.260}$, respectively.

Keywords: Porphyrin; Nickel complexes; Infrared spectra; Thermal analysis

1. Introduction

Photodynamic therapy (PDT) is a treatment that is used for the destruction of certain types of tumours [1]. It is well known that photodynamic therapy is based on the administration of a photosensitizer that concentrates in tumor cells and, upon subsequent irradiation with visible light in the presence of oxygen, selectively destroys the cancerous cells [2]. Photodynamic studies, in model systems and biological media carried out with a series of 5,10,15,20-tetrakis (methoxyphenyl) porphyrins, have shown that these synthetic porphyrins are effective photosensitizers that can be used as model compounds to investigate the effects of photosensitizers used in PDT [3–6]. Metalloporphyrins are widely studied because they play an important role in biology due to their crucial function in many biological processes like photosynthesis, biological red-ox reactions, and transport of oxygen. Among different metalloporphyrins, nickel (II) porphyrins are considered to be exemplary systems for spectroscopic studies because they display spectroscopic properties of theoretical interest [7]. At present, most work of porphyrin compound focus on the preparation technics, synthesis route and application. Preparation technics and application condition are restricted by thermal properties such as stability, melting temperature. However, there are surprisingly very little thermochemical data on 5,10,15,20-tetrakis (methoxyphenyl) porphyrin and their nickel metallo-complexes. In view of this, we studied the thermal behavior and thermal decomposition kinetics of this kind of porphyrins.

This paper reports the thermal stability, melting temperature, enthalpy of fusion and thermal decomposition kinetics of porphyrins and their nickel complexes. The thermal behavior at lower temperature including melting temperature and enthalpy of fusion has been investigated by differential scanning calorimetry technology and infrared spectra. The thermal stability and thermal decomposition kinetics have been studied by thermogravimetry.

* Corresponding author. Tel.: +86 27 67841856; fax: +86 27 67842752.
E-mail address: chendh46@hotmail.com (D. Chen).

0040-6031/$ – see front matter © 2005 Elsevier B.V. All rights reserved.
doi:10.1016/j.tca.2005.10.017

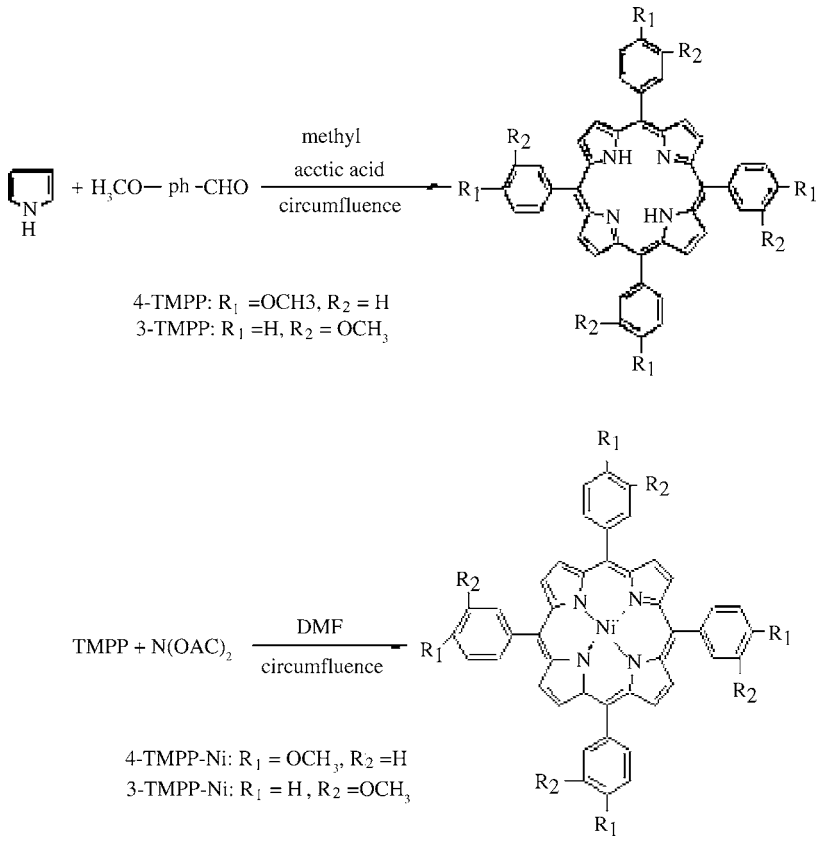

Scheme 1. The structures of the four samples.

2. Experimental

2.1. Materials

5,10,15,20-Tetrakis (4-methoxyphenyl) porphyrin (4-TMPP), 5,10,15,20-tetrakis (3-methoxyphenyl) porphyrin (3-TMPP), and their nickel metallo-complexes (4-TMPP-Ni and 3-TMPP-Ni) were synthesized by the method described in detail elsewhere [8,9]. Their structures were given in Scheme 1, which have been characterized by MS, ^{1}H NMR, FTIR and UV.

2.2. Differential scanning calorimetry (DSC) measurements

The thermal behaviors including melting temperature and enthalpy of fusion were determined with a computer controlled METTLER-TOLEDO DSC822^e (Co., Switzerland) under static air atmosphere. The temperature and energy of instruments had been calibrated by standard indium before all measurements. The reference pan was pure aluminum pan, which melt at 660 °C, so the highest measurement temperature is 600 °C. The thermal behavior of each specimen was investigated during first and second heating after cooling the sample from the melt at a cooling rate 10 °C min^{-1}. The DSC measurements on each sample were repeated twice and values agreed within the experimental uncertainties ±0.5 Jg^{-1} for the enthalpy of fusion and ±0.2 K for the melting temperature.

2.3. Thermogravimetry (TG) and FTIR spectra measurements

TG measurements were carried out on a TGS-2 thermal-balance (Perkin-Elmer Co., USA) in a static air atmosphere. Dynamic experiments were performed at several heating rates: 5, 8, 10, 15, and 20 °C min^{-1} with sample size ranging from 1.50 to 2.50 mg. The dynamic results presented in the paper were calculated from programs written by ourselves. According to the onset temperature of DTG curve to evaluate the onset decomposition temperature, sequentially estimate the thermal stability of the four samples. The infrared spectra (NICOLET-NEXUS 470 Co., USA) were recorded for samples of 3-TMPP and 3-TMPP-Ni at the given temperatures.

3. Theoretical consideration

3.1. Calculation of activation energy E_a by integral model-free method

The rate of solid-state non-isothermal decomposition reaction is expressed as

$$\frac{d\alpha}{dT} = \left(\frac{A}{\beta}\right) \exp\left(\frac{-E_a}{RT}\right) f(\alpha) \quad (1)$$

Rearranging Eq. (1) and integrating both sides of the equation leads to the following expression:

$$g(\alpha) = \left(\frac{A}{\beta}\right)\int_{T_0}^{T} \exp\left(\frac{-E_a}{RT}\right) dT \approx \left(\frac{A}{\beta}\right)\int_{0}^{T} \exp\left(\frac{-E_a}{RT}\right) dT = \left(\frac{AE_a}{\beta R}\right) P(u) \quad (2)$$

where $P(u) = \int_{\infty}^{u} -(e^{-u}/u^2)\,du$ and $u = E_a/RT$. Unfortunately, $P(u)$ cannot be analytically integrated. To solve this problem, an approximate formula [10] is introduced into Eq. (2). Taking the logarithms of both sides, Eq. (3) is obtained as

$$\ln\left(\frac{\beta}{T^{1.894661}}\right) = \ln\left[\frac{AE_a}{Rg(\alpha)}\right] + 3.635041 - 1.894661\,\ln E_a - \frac{1.001450E_a}{RT} \quad (3)$$

The plots of $\ln(\beta/T^{1.894661})$ versus $1/T$ give a group of straight lines. The activation energy E_a can be obtained from the slope $-1.001450\,E_a/R$ of the regression line.

3.2. Determination of the kinetic model by master plots method

Using a reference at point $\alpha = 0.5$ and according to Eq. (2), one gets

$$g(\alpha) = \left(\frac{AE_a}{\beta R}\right) P(u_{0.5}) \quad (4)$$

When Eq. (2) is divided by Eq. (4), the following equation is obtained:

$$\frac{g(\alpha)}{g(0.5)} = \frac{P(u)}{P(u_{0.5})} \quad (5)$$

Plots of $g(\alpha)/g(0.5)$ against α correspond to theoretical master plots of various $g(\alpha)$ functions [11,12]. To draw the experimental master plots of $P(u)/P(u_{0.5})$ against α from experimental data obtained under different heating rates, an approximate formula [13] of $P(u)$ with high accuracy was used $P(u) = \exp(-u)/[u(1.00198882u + 1.87391198)]$.

Eq. (5) indicates that, for a given α, the experimental value of $P(u)/P(u_{0.5})$ and theoretically calculated values of $g(\alpha)/g(0.5)$ are equivalent when an appropriate kinetic model is used. Comparing the experimental master plots with theoretical ones can conclude the kinetic model [14].

3.3. Estimation of the pre-exponential factor A and accommodate factor n

Experimental data, the expression of the kinetic model and the average activation energy predetermined are introduced into Eq. (2). The following expression is obtained:

$$\ln\left[\frac{\beta R}{E_a}\right] - \ln[P(u)] = \ln A - n\,\ln[g(\alpha)]^{1/n}$$

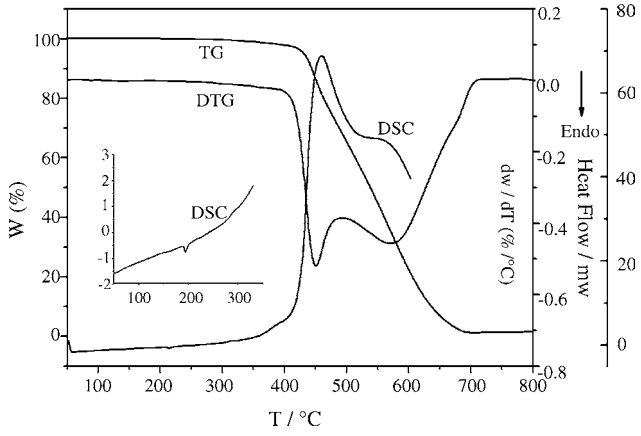

Fig. 1. TG/DTG and DSC curves for 4-TMPP with heating rate of 15 °C min^{-1} in air.

A group of lines were obtained by plotting $\ln[\beta R/E_a] - \ln[P(u)]$ against $-\ln[g(\alpha)]^{1/n}$. The logarithmic value of pre-exponential factor and the value of accommodate factor can be obtained from the interception and the slope, respectively.

4. Results and discussion

4.1. Thermal decomposition process

TGA is widely used for evaluating the thermal stability of samples because it requires a small sample and the entire study was over in a few hours. The TG/DTG and DSC curves of the four samples are shown in Figs. 1–4. The phenomenological aspects are illustrated in Table 1. From that we can see they are all stable up approximately 350 °C, which illustrate that all four samples have excellent stability. The DTG onset temperature follow the order 4-TMPP-Ni > 4-TMPP > 3-TMPP-Ni > 3-TMPP, which suggests that stability is 4-TMPP-Ni > 4-TMPP > 3-TMPP-Ni > 3-TMPP. The DTG peak temperature follow the order 3-TMPP-Ni > 4-TMPP-Ni > 3-TMPP > 4-TMPP, which different from the DTG onset temperature order. It may be because the thermal decomposition reaction rate ($d\alpha/dT$) of the four samples is greatly different at the same temperature.

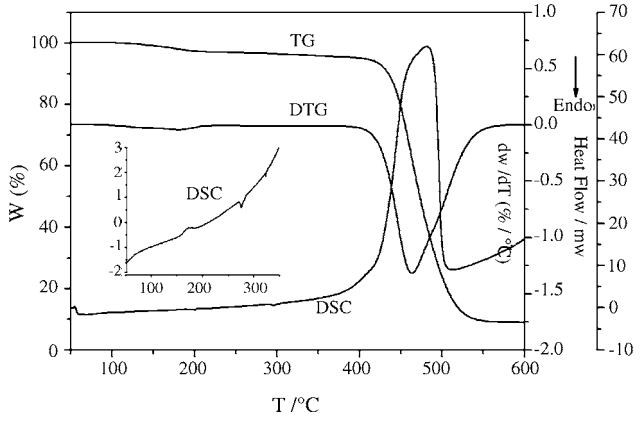

Fig. 2. TG/DTG and DSC curves for 4-TMPP-Ni with heating rate of 15 °C min^{-1} in air.

Table 1
Phenomenological data for the thermal decomposition of TMPP and TMPP-Ni in air ($\beta = 15\,^{\circ}C\,min^{-1}$)

Sample	Stage	TG plateaux (°C)	DTG peak (°C)	DSC peak (°C)	Mass loss (calculated, %)	Residue
4-TMPP	I	407–465	448	450	18.7 (16.9)	
	II	465–700	572		81.6 (83.1)	–
3-TMPP	I	365–474	453	454	16.7 (16.9)	
	II	474–650	597		84.1 (83.1)	–
4-TMPP-Ni	I	130–210	180	175	1.5	
	II	410–550	464	475	88.6 (90.5)	NiO
3-TMPP-Ni	I	375–610	480	486	88.1 (90.5)	NiO

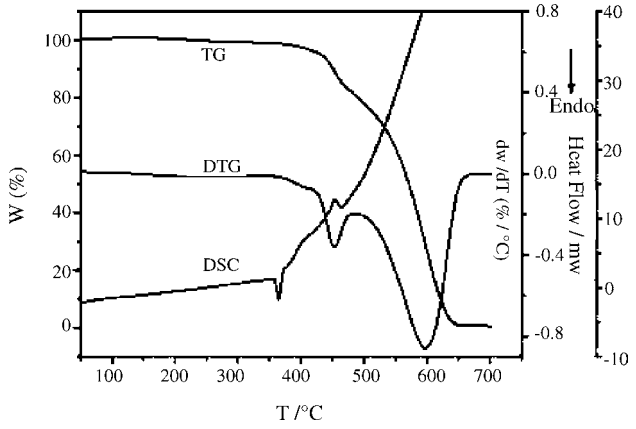

Fig. 3. TG/DTG and DSC curves for 3-TMPP with heating rate of 15 °C min^{-1} in air.

From the structures of these four samples, it also can be seen that the conjugative effect existing in the systems of 4-TMPP and 4-TMPP-Ni is better than that existing in the systems of 3-TMPP and 3-TMPP-Ni, which makes 4-TMPP and 4-TMPP-Ni have the better thermal stability than the other two.

Fig. 1 shows that the weight loss of 4-TMPP occurs in two steps; at the end of the decomposition almost no residue is remained. The initial weight loss (18.7%) observed between 407 and 465 °C is attributed to the remove of methoxy group (the theoretical value of 16.9%), correspondingly there is a 448 °C peak in DTG curve and 450 °C exothermic peak in DSC curve; after 465 °C until 700 °C, the mass loss reaches 100.3%, which is due to the complete disintegration of the intermediate. Similar phenomenon is observed in 3-TMPP.

Fig. 2 shows the TG/ DTG and DSC curves for 4-TMPP-Ni. The weight loss of 1.5% observed between 130 and 210 °C may be due to the elimination of small molecular impurity, which corresponds to the 180 °C peak in DTG curve and 175 °C exothermic peak in DSC curve. The evident weight loss of 88.6% is due to the complete decomposition of 4-TMPP-Ni and finally nickel oxide is remained (the theoretical value of 90.5%). 3-TMPP-Ni exhibits similar thermal decomposition process to that of 4-TMPP-Ni, but it contains no impurity.

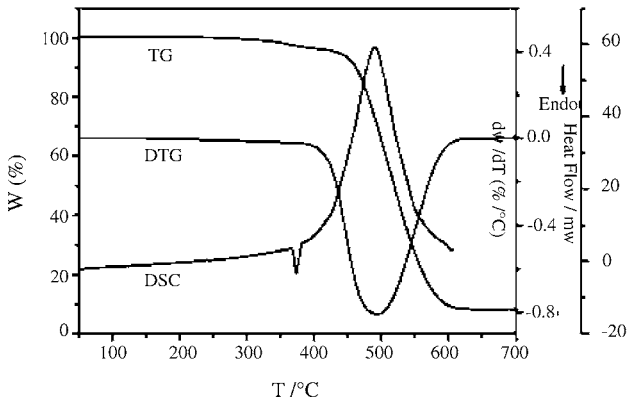

Fig. 4. TG/DTG and DSC curves for 3-TMPP-Ni with heating rate of 15 °C min^{-1} in air.

4.2. Thermal behavior at lower temperature

The thermal behavior at lower temperature obtained by DSC with the heating rate of 10 °C min^{-1} is shown in Figs. 5–8. The results obtained from DSC analysis are presented in Table 2. All the temperatures here represent the peak onset temperature of the DSC curves. The enthalpies (ΔH) are the thermodynamics parameter of these temperature variation processes, which were estimated from each DSC peak area computed by standard procedure in DSC apparatus, respectively.

As can be seen from the presented data, on heating and reheating 4-TMPP, an endothermic peak is observed at almost the same temperature; on cooling it from the given temperature, an exothermic peak is observed near the endothermic peak temper-

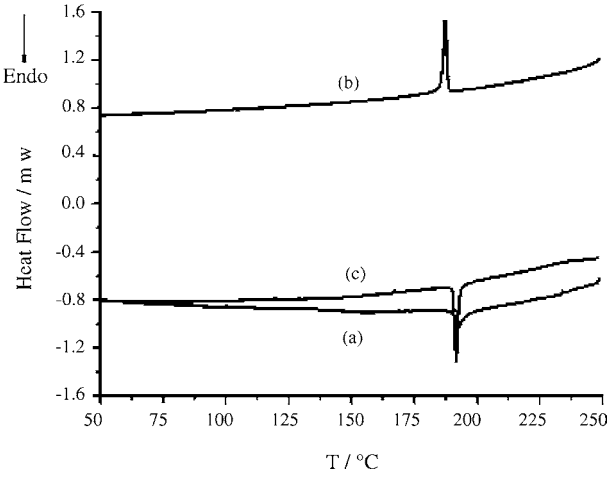

Fig. 5. DSC curves for 4-TMPP: (a) initial heating; (b) cooling; and (c) reheating the same sample (heating rate/cooling rate: 10 °C min^{-1}).

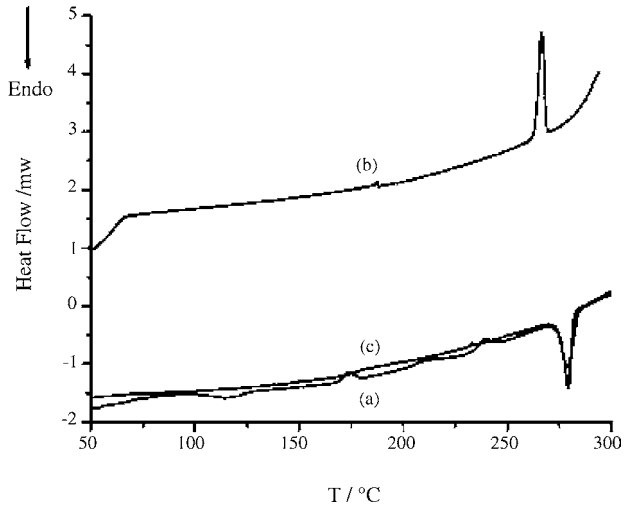

Fig. 6. DSC curves for 4-TMPP-Ni: (a) initial heating; (b) cooling; and (c) reheating the same sample (heating rate/cooling rate: 10 °C min^{-1}).

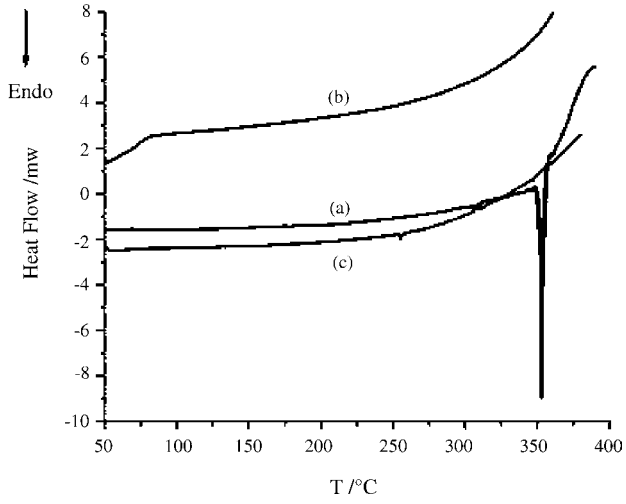

Fig. 7. DSC curves for 3-TMPP: (a) initial heating; (b) cooling; and (c) reheating the same sample (heating rate/cooling rate: 10 °C min^{-1}).

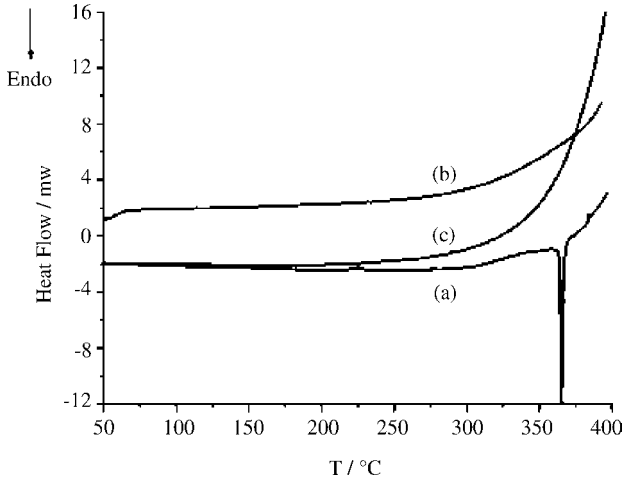

Fig. 8. DSC curves for 3-TMPP-Ni: (a) initial heating; (b) cooling; and (c) reheating the same sample (heating rate/cooling rate: 10 °C min^{-1}).

Table 2
Extrapolated onset temperature and enthalpy change of peak in DSC curve obtained by heating, cooling and reheating the samples

Sample	T_{on} (°C)/ΔH (J g^{-1})		
	Heating	Cooling	Reheating
4-TMPP	190.29/4.06	188.36/−7.06	190.47/7.78
4-TMPP-Ni	275.75/19.00	268.77/−19.57	274.94/19.66
3-TMPP	351.90/91.03	–	–
3-TMPP-Ni	363.97/79.81	–	–

ature; the enthalpy change (ΔH) observed on cooling is almost equal to that observed on reheating. In addition, the endothermic peak in the DSC curve has no corresponding change in the TG curve. Therefore, the endothermic peak observed in DSC curve can clearly be attributed to fusion of 4-TMPP. Similar phenomena are observed in 4-TMPP-Ni, but the melting point of 4-TMPP-Ni is higher than that of 4-TMPP.

Figs. 7 and 8 show that on heating 3-TMPP and 3-TMPP-Ni to 400 °C, a sharp endothermic peak is observed; on cooling and reheating, nothing is observed; after the endothermic peak DSC curve goes up rapidly. The results indicate that before the end of fusion the decomposition has already started, which can be confirmed by the infrared spectra (Figs. 9 and 10). The characteristic peaks in the IR spectra of 3-TMPP (Fig. 9) after heating to 300 °C is different from those of 3-TMPP heating to 360 °C. The weak absorption band (■) at 1235 cm^{-1} observed in Fig. 9a curve is assigned to the stretching vibration mode of ph–O, however it does not exist in Fig. 9b curve. The IR spectrum provides the evidence for the broken of ph–O bond before 360 °C. From Fig. 10, it also can be seen that the sharp absorption band (■) at 1229 cm^{-1} observed in Fig. 10a curve does not exist in Fig. 10b curve, which indicate that the ph–O bond has broken before 370 °C. Therefore, the decomposition temperature of 3-TMPP-Ni is between 350 and 370 °C. The results of IR analysis conform that the melting and decomposition processes of the two samples occur almost simultaneously.

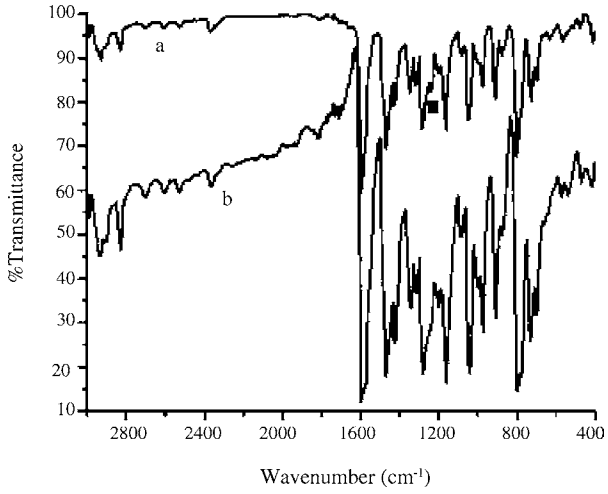

Fig. 9. FTIR spectra observed for 3-TMPP at: (a) 300 °C and (b) 360 °C.

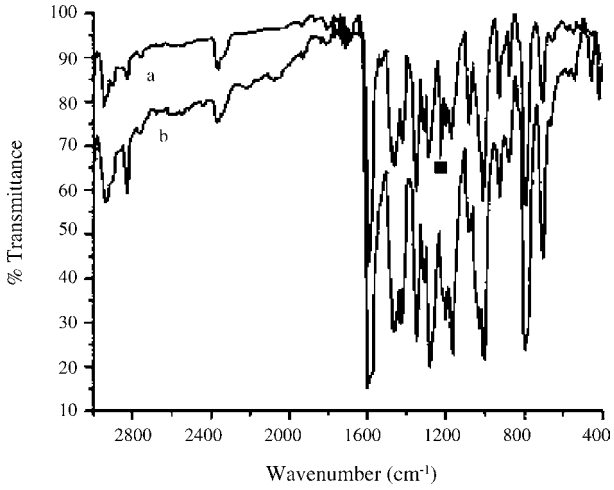

Fig. 10. FTIR spectra observed for 3-TMPP-Ni at: (a) 350 °C and (b) 370 °C.

Table 3
The activation energies of different extents of conversion

Conversion/α	Activation energies E_a (kJ mol^{-1})	
	4-TMPP-Ni	3-TMPP-Ni
0.2	113.16	113.27
0.3	117.01	116.90
0.4	121.01	118.61
0.5	125.22	122.17
0.6	129.68	121.75
0.7	134.56	123.54
0.8	140.03	125.86
Average	125.81	120.30

4.3. Kinetics analysis

4.3.1. Determination of activation energy E_a

The thermal decompositions of 4-TMPP-Ni and 3-TMPP-Ni are selected for the kinetic study. The TG curves of 4-TMPP-Ni and 3-TMPP-Ni at different heating rates are shown in Figs. 11 and 12, respectively. When $\alpha = 0.2$, 0.3, 0.4, 0.5, 0.6, 0.7, and 0.8, the corresponding activation energies are shown in Table 3. From Table 3 we can see that the activation energy

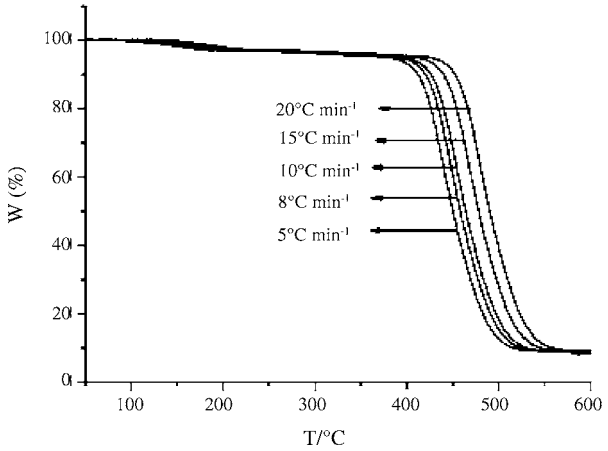

Fig. 11. TG curves of 4-TMPP-Ni at different heating rates in air.

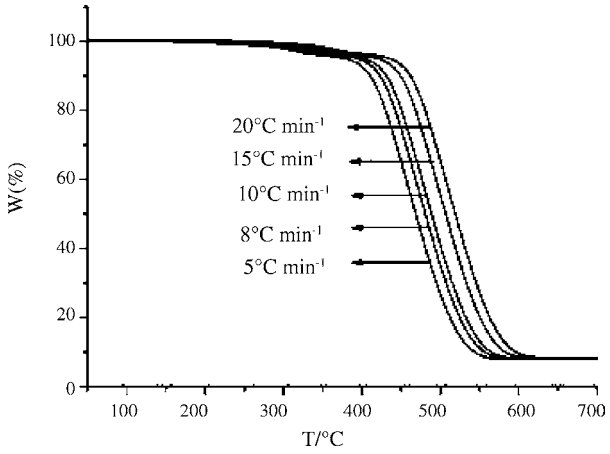

Fig. 12. TG curves of 3-TMPP-Ni at different heating rates in air.

hardly varies with the extent of conversion and the average activation energies are 125.81 and 120.30 kJ mol^{-1}, respectively. Little dependence of the activation energy on the extent of conversion indicates that there is a high probability for the presence of a single-step reaction.

4.3.2. Determination of kinetic model and estimation of pre-exponential factor A and accommodate factor n

The experimental master plots of $P(u)/P(u_{0.5})$ against α constructed from experimental data of the thermal decomposition of 4-TMPP-Ni under different heating rates and the theoretical master plots of various kinetic functions are all shown in Fig. 13. The experimental master plots of 3-TMPP-Ni and the theoretical master plots are shown in Fig. 14. The comparisons of the experimental master plots with theoretical ones indicate that the kinetic processes of the thermal decompositions of 4-TMPP-Ni and 3-TMPP-Ni are all most probably described by the A_m model, $g(\alpha) = [-\ln(1-\alpha)]^{1/m}$, because the experimental master plots lie between the theoretical master plots line 1 (A_4) and line 2 (A_3). The resulting logarithmic values of the pre-exponential

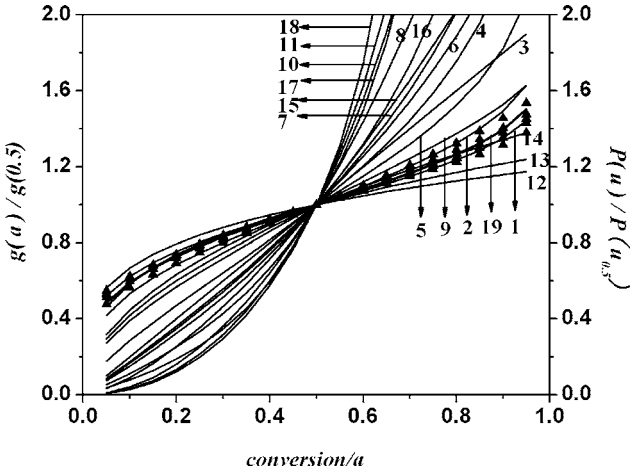

Fig. 13. Master plots of theoretical $g(\alpha)/g(0.5)$ against α for various reaction models (solid curves represent 18 kinds of reaction models, curve 19 represents function $g(\alpha) = [-\ln(1-\alpha)]^{0.278}$) and experimental data (▲) of 4-TMPP-Ni at the heating rates of 5, 8,10, 15, and 20 °C min^{-1}.

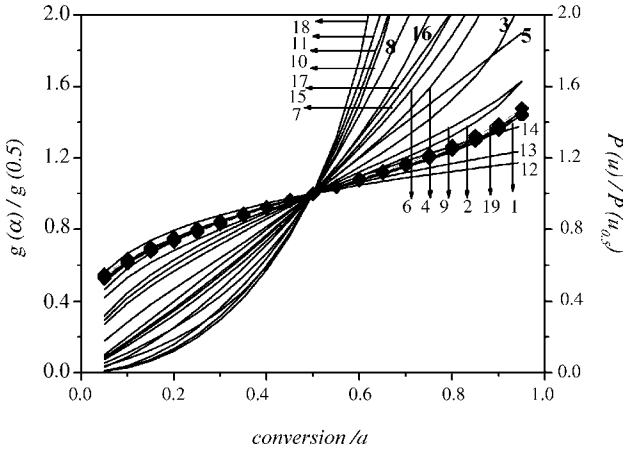

Fig. 14. Master plots of theoretical $g(\alpha)/g(0.5)$ against α for various reaction models (solid curves represent 18 kinds of reaction models, curve 19 represents function $g(\alpha) = [-\ln(1-\alpha)]^{0.260}$) and experimental data (♦) of 3-TMPP-Ni at the heating rates of 5, 8,10, 15, and 20 °C min^{-1}.

factor $\ln A$ (s^{-1}) are 12.671 and 18.219, the accommodate factors n (1/m) are 0.278 and 0.260, respectively.

5. Conclusions

4-TMPP and 4-TMPP-Ni exhibit higher thermal stability compared to 3-TMPP and 3-TMPP-Ni, but the melting point is much lower than that of 3-TMPP and 3-TMPP-Ni, TMPP-Ni exhibits higher thermal stability and melting point than that of the corresponding TMPP. For 3-TMPP and 3-TMPP-Ni, the melting and decomposition processes occur almost simultaneously. Both of the decomposition kinetic models of 4-TMPP-Ni and 3-TMPP-Ni follow nucleation and growth mechanism, Avrami-Erofeev equation with integral forms $g(\alpha) = [-\ln(1-\alpha)^{0.278}$ and $g(\alpha) = [-\ln(1-\alpha)^{0.260}$, respectively The activation energies E_a determined by integral model-free method are 125.81 and 120.30 kJ mol^{-1}. The resulting logarithmic values of the pre-exponential factor $\ln A$ (s^{-1}) are 12.671 and 18.219.

Acknowledgements

The financial support from the Key Natural Science Fund of Science and Technology Department of Hubei Province under grant no. 2001ABA009 for this work is greatly appreciated.

References

[1] K.C. Ackroyd, N. Brown, M. Reed, Photochem. Photobiol. 74 (2001) 656–669.
[2] M. La Penna, M. Gabriela Alvarez, E. Ines Yslas, Viviana Rivarola, E.N. Durantini, Dyes Pigments 49 (2001) 75–82.
[3] Z. Katona, A. Grofcsik, P. Baranyai, I. Bitter, G. Grabner, M. Kubinyi, et al., J. Mol. Struct. 450 (1998) 41–45.
[4] M.E. Milanesio, M.G. Alvarez, E.I. Yslas, C.D. Borsarelli, J.J. Silber, V. Rivarola, et al., Photochem. Photobiol. 74 (2001) 14–21.
[5] M. La Penna, M.G. Alvarez, E.I. Yslas, V. Rivarola, E.N. Durantini, Dyes Pigment 49 (2) (2001) 75–82.
[6] I. Yslas, M.G. Alvarez, C. Marty, G. Mori, E.N. Durantini, V. Rivarola, Toxicology 149 (2000) 69–74.
[7] P. Serguei, M.K. Pawel, Z.Z. Marek, J. Chem. Phys. 121 (2004) 3.
[8] A.D. Adler, F.R. Longo, J.D. Finarelli, J. Goldmacher, J. Assour, L. Korsakoff, J. Org. Chem. 32 (1967) 476.
[9] A.D. Adler, F.R. Longo, F. Kampas, J. Kim, J. Inorg. Nucl. Chem. 32 (1970) 2443.
[10] T. Wanjun, L. Yuwen, Z. Hen, W. Cunxin, Thermochim. Acta 408 (2003) 39.
[11] F.J. Gotor, J.M. Criado, J. Malek, N. Koga, J. Phys. Chem. A 104 (2000) 10777.
[12] L.A. Perez-Maqueda, J.M. Criado, F.J. Gotor, J. Malek, J. Phys. Chem. A 106 (2002) 2862.
[13] T. Wanjun, L. Yuwen, Z. Hen, W. Zhiyong, W. Cunxin, J. Therm. Anal. Cal. 74 (2003) 309.
[14] W. Tang, Y. Liu, X. Yang, C. Wang, Ind. Eng. Chem. Res. 43 (2004) 2054–2059.